university of groningen

University Medical Center Groningen

University of Groningen

Mass transfer in rolling rotary kilns

Heydenrych, M.D.; Greeff, P.; Heesink, A. Bert M.; Versteeg, G.F.

Published in:
Chemical Engineering Science

DOI:
10.1016/S0009-2509(02)00312-3

IMPORTANT NOTE: You are advised to consult the publisher's version (publisher's PDF) if you wish to cite from it. Please check the document version below.

Document Version
Publisher's PDF, also known as Version of record

Publication date:
2002

Link to publication in University of Groningen/UMCG research database

Citation for published version (APA):
Heydenrych, M. D., Greeff, P., Heesink, A. B. M., & Versteeg, G. F. (2002). Mass transfer in rolling rotary kilns: a novel approach. *Chemical Engineering Science*, *57*(18), 3851-3859. https://doi.org/10.1016/S0009-2509(02)00312-3

Copyright
Other than for strictly personal use, it is not permitted to download or to forward/distribute the text or part of it without the consent of the author(s) and/or copyright holder(s), unless the work is under an open content license (like Creative Commons).

The publication may also be distributed here under the terms of Article 25fa of the Dutch Copyright Act, indicated by the "Taverne" license. More information can be found on the University of Groningen website: https://www.rug.nl/library/open-access/self-archiving-pure/taverne-amendment.

Take-down policy
If you believe that this document breaches copyright please contact us providing details, and we will remove access to the work immediately and investigate your claim.

Downloaded from the University of Groningen/UMCG research database (Pure): http://www.rug.nl/research/portal. For technical reasons the number of authors shown on this cover page is limited to 10 maximum.

Download date: 05-05-2023

PERGAMON

Chemical Engineering Science 57 (2002) 3851–3859

Chemical Engineering Science

www.elsevier.com/locate/ces

Mass transfer in rolling rotary kilns: a novel approach

M. D. Heydenrych[a,*], P. Greeff[a], A. B. M. Heesink[b], G. F. Versteeg[b]

[a] *Department of Chemical Engineering, University of Pretoria, Pretoria, South Africa*
[b] *Department of Chemical Technology, University of Twente, Enschede, The Netherlands*

Received 29 November 2001; received in revised form 3 June 2002; accepted 23 June 2002

Abstract

A novel approach to modeling mass transfer in rotary kilns or rotating cylinders is explored. The movement of gas in the interparticle voids in the bed of the kiln is considered, where particles move concentrically with the geometry of the kiln and gas is entrained by these particles. The approach considers a differential section along the length of a rotary kiln where the gas concentration in the freeboard is assumed to be uniform in that section. A reactor modelling approach has been used to derive effectiveness factors for the bed as a function of bed fill, reaction kinetics and rotation speed. In many cases, the entrained gas becomes depleted within the bed, leading to a simplified model for the bed effectiveness factor. Experimental data confirms the validity of this model for slower rates. At faster rates, mass transfer can be much higher than the model predicts, indicating that other mechanisms, such as dispersion or diffusion are also important in these conditions.
© 2002 Elsevier Science Ltd. All rights reserved.

Keywords: Rotating drum; Reaction engineering; Drying; Convective transport; Granular materials; Passive layer

1. Introduction

Rotary kilns are used industrially in many applications such as drying, incineration, mixing, pre-heating, humidification, calcining, reducing, sintering and gas–solid reactions (Barr, Brimacombe, & Watkinson, 1989; Jauhari, Gray & Masliya, 1998).

For many rotary kilns, heat transfer is the limiting factor, both in the heating section of the rotary kiln, and in the reaction zone (Barr et al., 1989, Tscheng and Watkinson, 1979). Consequently, most focus in the literature has been directed at understanding the heat transfer processes in rotary kilns. It is important though to understand all of the processes that occur in rotary kilns on a fundamental level before rotary kilns can be designed and operated optimally.

With physical processes like drying and humidification for example, mass transfer is also important, as well as in gas–solid reacting systems with high specific reaction rates such as incineration. In this work, we will examine the mass transfer in rolling rotary kilns and propose a novel approach to describe the phenomena that determine the rate of mass transfer.

2. Modelling studies

The first published experimental studies on rotary kilns recorded the relationship of rotation speed and kiln inclination on bed depth and solids residence time (Sullivan, Maier, Ralston, 1927). A model was later developed based on the assumption that particles in a rolling bed move in a circular motion with the rotation of the kiln, and then fall down the surface of the bed in a thin layer (Saeman, 1951). The time taken to fall down the surface was assumed to be small compared to the time for a particle to move with the kiln from the bottom half to the top half of the bed. Using the geometry of an inclined rotary kiln, the angle of inclination necessary to maintain a constant bed height over the length of the rotary kiln could be determined for a given rotation speed. This basic model predicted the original data (Sullivan et al., 1927) well, and the model was further refined to predict axial movement of particles with different bed fills, taking into account the time for particles to fall down the surface of the bed (Kramers & Crookewit, 1952). In later work that specifically measured the movement of

* Corresponding author. Tel.: +27-12-420-2199; fax: +27-12-660-1518.
E-mail address: mike@heydenrych.info (M. D. Heydenrych).

0009-2509/02/$ - see front matter © 2002 Elsevier Science Ltd. All rights reserved.
PII: S0009-2509(02)00312-3

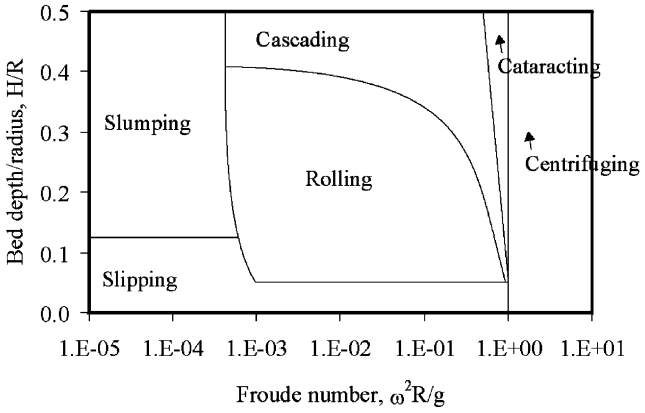

Fig. 1. An example of a bed behaviour diagram (Heinen et al., 1983a).

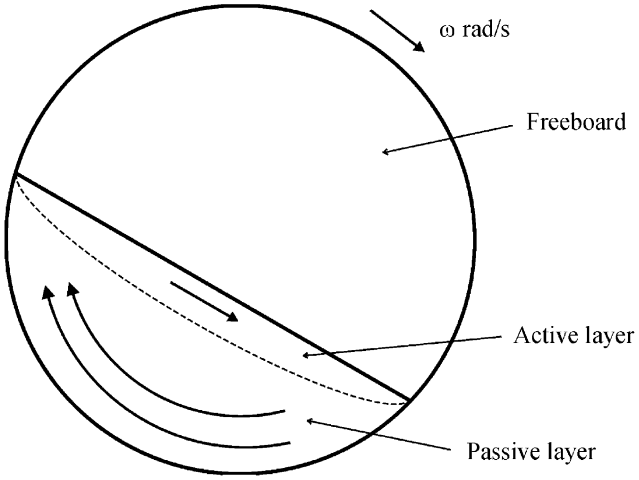

Fig. 2. The various zones within a rotary kiln.

particles at the surface of the kiln, the validity of the model of Kramers and Crookewit (1952), with minor exceptions, was confirmed (Lebas, Hanrot, Ablitzer, & Houzelot, 1995). More recently, the same fundamental model of the path of particles was shown to be correct in a study of particle motion where there is no net axial flow of particles in a rotating drum (Spurling, Davidson, & Scott, 2000).

The conditions that determine the mode in which a rotary kiln operates—slipping, slumping, rolling, cascading, cataracting, centrifuging—have been extensively examined, and can be represented using a bed behaviour diagram (Heinen, Brimacombe, & Watkinson, 1983b). An example of a bed behaviour diagram is shown in Fig. 1. In this paper, we will focus on kilns operating in the preferred mode for most circumstances—rolling.

The time for a colored particle to move down the surface of the bed was measured with video photography (Lebas et al., 1995), and this typically takes 15–30% of a full cycle. However, this ratio does not change with rotation speed, and the velocity of the particles moving down the surface of the bed was interpreted to be directly proportional to rotation speed (Lebas et al., 1995).

The layer of particles moving down the face of the bed leads to improved mass transfer, therefore the surface layer is often referred to as the "active layer" (see Figs. 2–5). Heinen et al. (1983a) measured particle velocities inside this layer as well as the thickness of it, and found that it is relatively thin for beds with a depth that is much larger than the diameter of the particles. In most cases, the active layer is typically less than eight particle diameters deep, except for deep beds with small particles, where the depth of the active layer is less than 12% of the bed depth, falling to as low as 4% for slowly rotating kilns (Heinen et al., 1983a).

3. Model development

For most of the volume of the bed of a rotary kiln (the passive layer), particles move concentrically with the wall of the bed, with no slippage between particles. As the particles approach the bed surface due to the kiln rotation, they slip down the face of the bed, and come to rest near the bottom

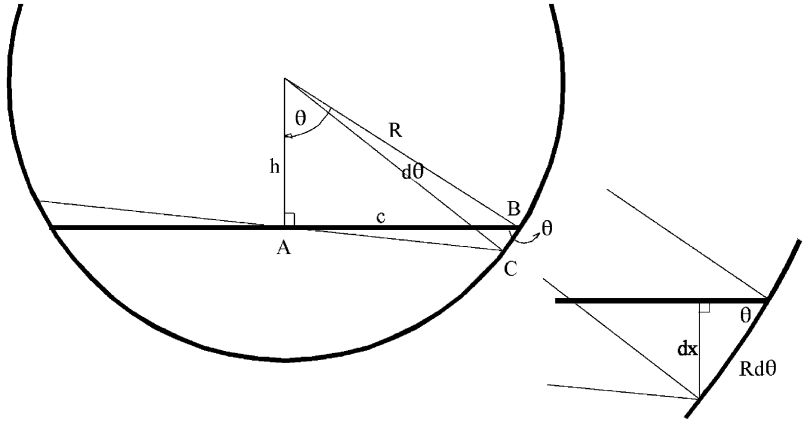

Fig. 3. Overall displacement of particles at the surface of a kiln (irrespective of the path). Note that the bed surface will normally be inclined, but for convenience has been drawn horizontally.

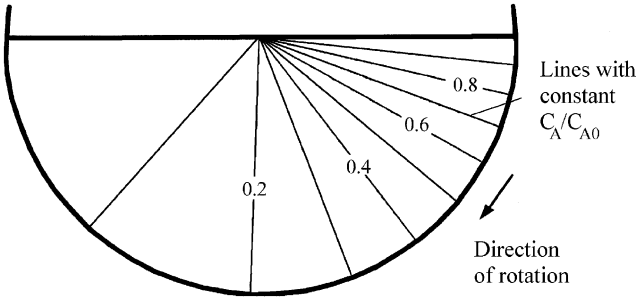

Fig. 4. For a half-filled kiln, the residence time at any radius is equal, yielding concentration profiles shown here for a first-order reaction with $k/\omega = 1$. The lines are calculated using $C_A/C_{A0} = e^{-(k/\omega)\theta}$.

of the surface of the bed. We will attempt to quantify the volumetric flow rate and reaction rate of the gas that is trapped in the interparticle voids in the passive layer.

3.1. Gas volumetric flow rate

The volume of entrained gas can be determined for a single rotation of the kiln (for convenience, the bed has been represented horizontally):

The differential area within ABC can be approximated by $\frac{1}{2}$ base $\times$ perpendicular height. The perpendicular height dx can be found as follows:

$$dx = (\sin\theta)R\,d\theta = (c/R)R\,d\theta = c\,d\theta, \quad (1)$$

$$dA_x = \tfrac{1}{2}c\,dx = \tfrac{1}{2}c^2\,d\theta. \quad (2)$$

The area useful for the entrainment of gas is proportional to the void fraction of gas in the bed

$$dA_{xg} = \frac{\varepsilon}{2}(R^2 - h^2)\,d\theta. \quad (3)$$

Integrating this expression over 1 rad, and converting to angular velocity, the volume flow rate of gas is

$$Q = \tfrac{1}{2}\varepsilon\omega L(R^2 - h^2). \quad (4)$$

This gives the volume flow rate of entrained gas through the bed of a rotary kiln. By estimating the concentration of the gas as it leaves the bed, the overall reaction rate can be determined.

To understand how the active layer influences the movement of gas, consider a line extending from the radial centre of the kiln, passing perpendicularly through the bed surface to the deepest part of the bed. All entrained gas will pass this line. If the active layer is infinitely thin, the flow rate Q can easily be shown to be as in Eq. (4). A mass balance of the particles also means that the particles will move infinitely fast over the surface of the bed with the assumption of an infinitely thin active layer. In practice, the particles will move down at a finite velocity, with a finite active layer thickness. However, for the purposes of this paper, the admittedly unrealistic assumption of an infinitely thin layer, not affecting the entrainment of gas perpendicular to the bed surface, will be taken through to its conclusion.

3.2. Nature of concentration profiles within the bed

The movement of the gas in the voids is assumed to be a circular arc, following the geometry of the kiln, until the gas reaches the surface of the bed again (Saeman, 1951). *For a half-filled kiln*, the retention time of such gas will be the same, regardless of the radius of the arc. Furthermore, this retention time for the half-full kiln will be the time it takes for half of a revolution: $\tau = \pi/\omega$. If we assume that the gas following this path will move in plug flow, we can expect a concentration profile fitting an exponential decay. Therefore, we can expect the concentration profile within the bed of a rotary kiln to be as in Fig. 4.

Diffusion and dispersion will no doubt play a role in the kiln, especially in the centre of the kiln, where several concentrations converge. In this part, the effect of the active layer will be important, and dispersion effects will predominate. The inclusion of dispersion will require a more complex model, not discussed here.

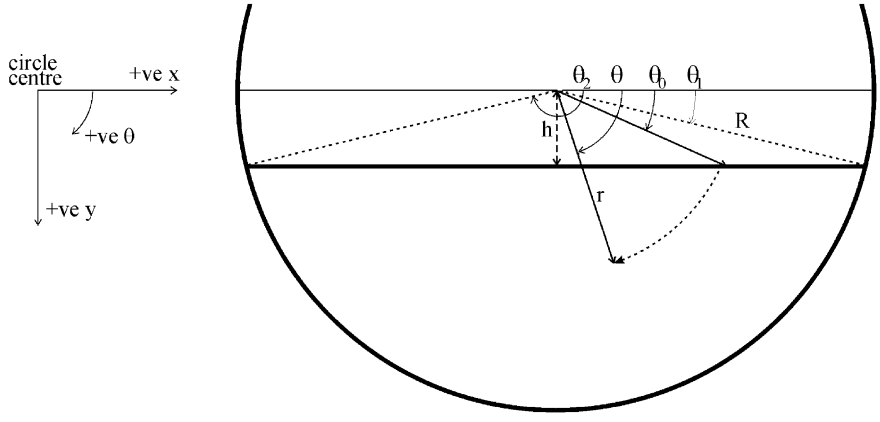

Fig. 5. Definition of angles for determination of iso-residence time lines.

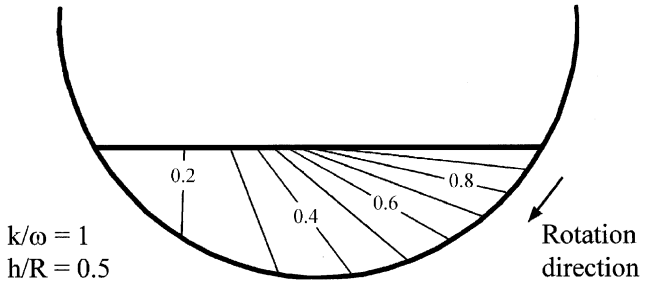

Fig. 6. Concentration profiles for $k/\omega = 1$ at C_A/C_{A0} intervals of 0.1.

For bed fills of less than 50%, the residence time at each radius will be different, and the expected concentration profiles can be calculated:

$$\tau(\theta, r) = \frac{\theta - \theta_0}{\omega} = \frac{\theta - \sin^{-1}(h/r)}{\omega}. \tag{5}$$

Further simplifying and converting to rectangular coordinates shows that constant residence times form straight lines:

$$y = x\tan(\omega\tau) + \frac{h}{\cos(\omega\tau)}. \tag{6}$$

This applies to any reaction kinetics, and different reaction kinetics will simply determine the spacing of the lines. As an example, let us consider a first-order reaction,

$$-P_A = \varepsilon k C_A, \tag{7}$$

where P_A is the reaction rate of A per unit of bed volume and k is the reaction rate constant with respect to the gas phase, with units of s^{-1}. Because C_A necessarily refers to moles per m^3 of gas, we multiply by the bed voidage to get P_A in terms of total bed volume. Then

$$k\tau = -\ln\left(\frac{C_A}{C_{A0}}\right). \tag{8}$$

Substitute τ into Eq. (6) for first-order iso-concentration lines, shown in Fig. 6.

In this paper, a model is developed for reaction rates based on the volume of the bed. The rate constant k is defined as a reaction rate constant for a reaction occurring on the surface of the particles, assuming that there are no mass transfer limitations occurring. In the experimental section of this paper, there are two other situations that determine the effective rate, and these are both mass transfer limiting situations:

- where mass transfer from the interparticle voids to the surface of the particles is limiting, and
- where mass transfer within the intraparticle voids is limiting (using a shrinking core model).

In each of these situations, the mass transfer coefficient has been rewritten in a form that replaces the reaction rate constant k (Eqs. (20) and (24), respectively). The reaction rate model being developed here is thus used as a generalised form of expressing the rate at which reaction or mass transfer (e.g. drying) takes place.

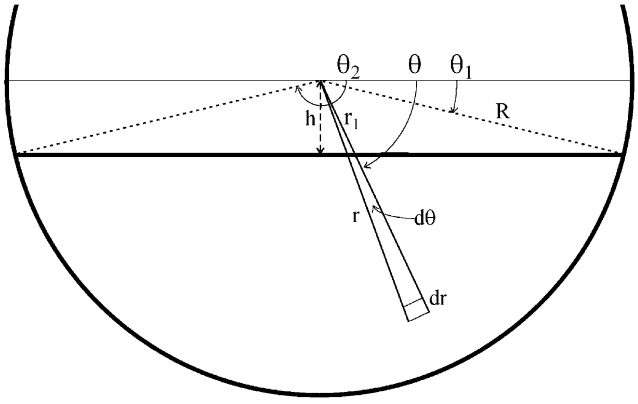

Fig. 7. Definition of variables used in Eqs. (9)–(12).

3.3. Effectiveness factors

For convenience, such concentration profiles through the bed can rather be expressed by an effectiveness factor. This factor is defined as the ratio of the actual rate of the reaction over the bed to the rate that would be obtained if the whole bed were exposed to gas at the highest gas concentration—the concentration above the bed.

In the general case of kilns with a given fill, actual rate is the average rate over the entire cross-sectional area (see Fig. 7).

$$\int_V P_A(r,\theta,z)\,\mathrm{d}V_{\mathrm{bed}} = \left[\int_{\theta_1}^{\theta_2}\int_{r_1}^{R} \varepsilon k C_{A0} \mathrm{e}^{-(k/\omega)}(\theta - \sin^{-1}(h/r))r\,\mathrm{d}r\,\mathrm{d}\theta\right]\mathrm{d}z, \tag{9}$$

$$\theta_1 = \sin^{-1}(h/R), \quad \theta_2 = \pi - \sin^{-1}(h/R),$$
$$r_1 = h/\sin\theta. \tag{10}$$

From the definition of the effectiveness factor and realising that the cross-sectional area of the bed equals $\frac{1}{2}R^2(\theta_2 - \theta_1 - \sin(\theta_2 - \theta_1))$,

$$\eta = \frac{\int P_A(r,\theta,z)\,\mathrm{d}V_{\mathrm{bed}}}{\varepsilon k C_{A0} V_{\mathrm{bed}}}, \tag{11}$$

$$\eta = \frac{2}{R^2(\theta_2 - \theta_1 - \sin(\theta_2 - \theta_1))} \times \int_{\theta_1}^{\theta_2}\int_{r_1}^{R} \mathrm{e}^{(k/\omega)(\theta - \sin^{-1}(h/r))} r\,\mathrm{d}r\,\mathrm{d}\theta. \tag{12}$$

This function is represented graphically in Figs. 8 for different bed fillings as a function of the k/ω ratio. It is interesting to note that the size of the rotary kiln is irrelevant using this model. The only variables in this model are the bed fill and k/ω. Later in the paper, we will discuss the role of other parameters that are dependent on the scale of the rotary kiln.

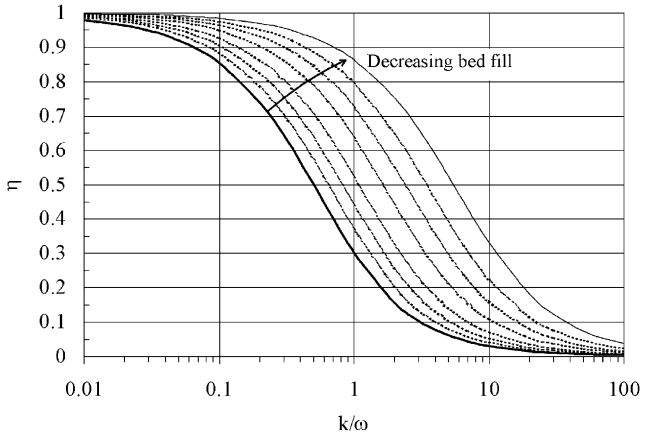

Fig. 8. Effectiveness factors increase as bed fill decreases, and are independent of bed radius R. Fill fractions shown are 0.5 (solid line), 0.37, 0.25, 0.14, 0.052, 0.019, 0.007 and 0.0017 (thin line).

As expected, for a given k/ω, the effectiveness increases for shallower beds.

For the special case of a half-filled cylinder, $h = 0$:

$$\eta = \frac{2}{\pi R^2}\int_0^{\pi}\int_0^{R} r e^{-(k/\omega)\theta}\,dr\,d\theta \tag{13}$$

$$= \frac{\omega}{k\pi}(1 - e^{-k\pi/\omega}). \tag{14}$$

This is also easily derived from first principles. By taking a mole balance for a given volume of bed, where C_A is the concentration of gas leaving the bed,

$$\int_V -P_A\,dV_{bed} = Q(C_{A0} - C_A). \tag{15}$$

Substituting for P_A from Eq. (7) and for Q from Eq. (4) gives the same result as Eq. (14).

4. Total depletion model

The double integral of Eq. (13) is cumbersome to work with; a simplified approach for estimating η would be more useful. For high k/ω values such a simple approach is quite possible.

For high k/ω, the gas leaving the system at the surface of the bed can be assumed to be fully depleted (or saturated, in the case of drying). In this case, we assume complete reaction and use Eq. (4) to estimate the volume flow rate of entrained gas.

Choosing 95% conversion as the criterion, $C_A/C_{A0} = 0.05$, and this gives the approximation of the Damköhler number $k\tau = 3$. For a half-filled kiln, all paths through the kiln have the same residence time, and $\tau = \pi/\omega$. For lesser fill fractions, we will choose $\frac{1}{2}$ of the maximum angle. With this basis, a criterion for using the simplified model can be derived:

$$\frac{k}{\omega} > \frac{3}{\cos^{-1}(h/R)}. \tag{16}$$

Using an effectiveness factor and assuming total conversion gives

$$\eta = \frac{\omega}{2kA_x}(R^2 - h^2). \tag{17}$$

Noting that the term $(R^2 - h^2)/A_x$ is dimensionless, an effectiveness factor can again be calculated as a function of k/ω and h/R, this time using Eq. (17). In Table 1, the effectiveness factors obtained using Eqs. (12) and (17) are compared at the criterion given by Eq. (16).

5. Model validation

5.1. Literature data

Jauhari et al. (1998) measured mass transfer in a rotating drum by measuring the evaporation rate of decane from impregnated alumina particles. Most of the measurements were done using shallow beds with baffles (flights) fitted to the rotary kiln. This gives rise to a geometry that is not well described by the model in this paper. However, one set of data was reported for a shallow rolling bed (4.3% fill), and only this set of data will be used here.

Mass transfer rates were measured for various kiln conditions, assuming an ideally mixed gas phase. The results were expressed in the form of a volumetric mass transfer coefficient k_sA/V_{bed}, defined as

$$QC_{decane,out} = \frac{k_sA}{V_{bed}}(C_{decane,sat} - C_{decane,out})\,V_{bed}. \tag{18}$$

We can make use of the k_sA/V_{bed} data by comparing those with the equivalent data predicted by our model:

$$QC_{decane,out} = \int P_{decane}\,dV_{bed}$$

$$= \eta\varepsilon k(C_{decane,sat} - C_{decane,out})V_{bed}. \tag{19}$$

As mass transfer from the surface of the alumina particles is the rate determining step (as long as the pores are sufficiently filled), the first-order reaction rate constant (with respect to the gas phase), follows from

$$k = \frac{k_{gs}a}{\varepsilon} = \frac{6k_{gs}(1-\varepsilon)}{d_p\varepsilon} \tag{20}$$

with k_{gs} being the mass transfer coefficient at the surface of the alumina particles. We should thus compare the k_sA/V_{bed} data of Jauhari et al., with the $6\eta k_{gs}(1-\varepsilon)/d_p$ data that we can produce with our model using Eq. (12) or (17). Before doing so, we must find an appropriate value for k_{gs}. For that purpose, we use the findings of Sørensen and Stewart (1974) who studied mass transfer in packed beds. For a stagnant fluid they derived:

$$k_{gs} = \frac{ShD}{d_p} \quad \text{with } Sh = 3.8. \tag{21}$$

Table 1
The error caused by using the simplified model at the criterion values is less than 6% in all relevant cases

h/R	Fill fraction	k/ω	η (Eq. (12))	η, Total depletion model (Eq. (17))	Error (%)
0	0.5	1.91	0.164	0.1667	1.65
0.2	0.374	2.19	0.1849	0.1867	0.97
0.4	0.252	2.59	0.2006	0.2047	2.09
0.6	0.142	3.24	0.214	0.2211	3.33
0.8	0.052	4.66	0.2259	0.2361	4.56
0.9	0.0187	6.65	0.2313	0.2432	5.16
0.95	0.00666	9.45	0.2338	0.2466	5.45
0.98	0.00169	14.97	0.2354	0.2487	5.63

Table 2
Conditions used in our model

Total volume	20.3 l
Bed volume	0.875 l
h/R	0.824
R	0.145 m
h	0.1195 m
Cross-sectional bed area (A_x)	0.00284 m^2
Particle diameter (d_p)	3×10^{-3} m
Binary diffusion coefficient of decane in nitrogen at 20°C (D_{ab})	6×10^{-6} m^2 s^{-1}
Interparticle voidage (ε)	0.45 (assumed)
Sherwood number (Sh)	3.8
Gas–solid mass transfer coeff. (k_{gs})	7.6×10^{-3} m s^{-1}
k	$(6k_{gs}(1-\varepsilon)/\varepsilon d_p =)18.6$ s^{-1}

As the gas entrained into the bed of a kiln is regarded to have no slip velocity with regard to the particles in the bed, and the bed porosity is comparable to that of a packed bed, Eq. (21) is assumed to be appropriate.

If we now apply the precise conditions at which Jauhari et al., have produced their k_sA/V_{bed} data, we are able to calculate the corresponding $6\eta k_{gs}(1-\varepsilon)/d_p$ data with our model. These conditions are summarised in Table 2.

Table 3 compares our results with the data measured by Jauhari et al. (1998). In all cases, k/ω is much higher than the value of the criterion given by Eq. (16) (i.e. $k/\omega > 5$), meaning that saturation is easily reached within the bed, and that the mass transfer contribution by the convective model is practically insensitive to the calculated rate constant k. The value of $\eta\varepsilon k$ can therefore be calculated with little error using Eq. (17). Fig. 9 shows the comparison of the experimental data of Jauhari et al. (1998), given by k_sA/V_{bed} with our own model, given by $\eta\varepsilon k$.

The fact that the mass transfer rates measured by Jauhari et al. (1998) are so much higher than the model given by Eq. (17) can only be ascribed to a great deal of evaporation taking place at the surface of the bed. In the active layer, with wet particles, there is bound to be a significant amount of evaporation taking place directly into the freeboard gas, and this evaporation will also depend on the velocity of the freeboard gas axially along the kiln. For suitable conditions to test the passive layer model, the rate of evaporation should preferably not be influenced by the freeboard gas velocity. This happens when the rate of evaporation is determined by the diffusion of vapour through the outer layers of a porous particle, and it was with this in mind that the following experiments were designed.

5.2. Measured data

In order to test our model at conditions where kinetics are much slower, we performed similar experiments to Jauhari et al., but using larger particles, allowing the evaporation to continue until the particles were dry. In this way, mass transfer within the pores of the particles became the rate limiting process in the final drying stage.

The rotating drum used has a diameter of 0.15m and a length of just 0.041 m (Fig. 10). It is made of steel with a polycarbonate observation window. It was only operated in the rolling mode at two speeds: 0.052 and 0.266 rad/s. Air was introduced through a rotameter and blown through a 1 mm jet directly away from the bed towards the circular wall of the rotating drum, in order to ensure good mixing of the gas above the bed and to prevent any bypassing of gas to the central exit. Like Jauhari et al. (1998), hydrocarbon concentration was measured continuously using a sensor. The sensor was calibrated so that the sensor reading could be transformed to a linear hydrocarbon concentration reading. Because the hydrocarbon concentration and air flow rate were known at all times during a run, it was possible to calculate what fraction of hydrocarbon liquid had evaporated at any time. The fraction of liquid remaining in the particle (liquid loading, z) has been used as a parameter to characterise the particle at a given set of conditions.

The experimental technique to measure mass transfer rates differs from that used by Jauhari et al., because the sensor was placed within the rotating drum, near the gas exit. This allowed us to directly measure the build-up of concentration within the freeboard gas after the gas flow had been stopped.

Table 3
Comparison of measured data and model predictions

Rotation speed N (rpm) (rpm)	Angular velocity ω (s^{-1})	Measured data k_sA/V_{bed} (s^{-1})	k/ω	$\eta\varepsilon k$ (Eq. (17)) (s^{-1})
0.29	0.031	0.121	612	0.0164
0.59	0.062	0.198	301	0.0329
1.23	0.128	0.411	144	0.0685
1.67	0.175	0.502	106	0.0933
1.97	0.206	0.604	90	0.1101

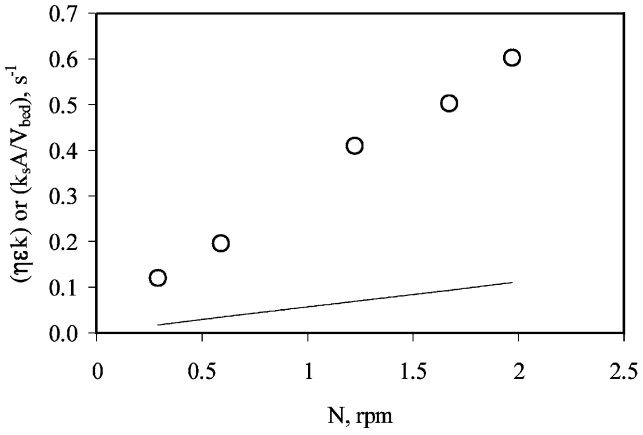

Fig. 9. Mass transfer data measured by Jauhari et al., is significantly higher than that predicted by our model: (—) $\eta\varepsilon k$ from Eq. (17), (o) k_sA/V_{bed} for 0.043 fill (Jauhari et al.).

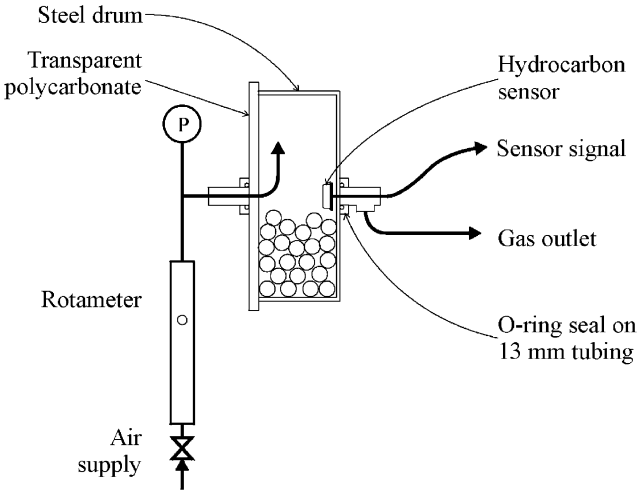

Fig. 10. Flow diagram of experimental apparatus.

For the experiments reported here, we used spherical tab-alumina particles of average diameter 16 ± 1 mm soaked in 1-pentanol. The 44 pellets that were used gave an average fill fraction of 0.27. The particles were wiped dry before being loaded in the rotating drum. During the experiment, air flowed through the rotating drum. At suitable intervals, the gas flow was stopped, and the rate of increase of hydrocarbon concentration was measured until it came close to saturation. Good mixing of the gas within the freeboard was assumed, due to the continuous rotation of the walls and the movement of the particles at the top of the bed. The rate at which the gas in the freeboard was saturated characterised the rate of mass transfer of the hydrocarbon from the pellets to the freeboard. The characteristic rate of the system ($\eta\varepsilon k$, see Eq. (19)) was therefore calculated from the exponential rise in the hydrocarbon concentration in the freeboard as a function of time

$$\eta\varepsilon k(C_{sat}-C)V_{bed}=V_f\frac{dC}{dt}, \tag{22}$$

which can be integrated to give

$$-\ln\left(\frac{C_{sat}-C}{C_{sat}-C_0}\right)=\frac{V_{bed}}{V_f}\eta\varepsilon k\cdot t. \tag{23}$$

C_{sat} could be accurately estimated by visually noting how the end points of the graph of $-\ln((C_{sat}-C)/(C_{sat}-C_0))$ vs. t fitted the straight line formed by the other points. An example of such a graph is given in Fig. 11.

For every experiment when the air flow was stopped to measure the rate of saturation of the freeboard gas, C_{sat} was recalculated. Several such measurements were performed during a run (with liquid loading of the particles decreasing continuously), using both fast and slow rotation speeds. The saturation concentrations inferred with this technique did not vary substantially during the run, as can sometimes happen with small pores, or when desorption within the particles becomes rate limiting. The saturation concentrations determined in this way varied by less than 1% throughout a run.

We used a similar technique to model the characteristic rate of the system ($\eta\varepsilon k$) as with Jauhari's data, except that we now added a shrinking core model to the resistance term. The term z is liquid loading, and ε_{part} is the intraparticle porosity:

$$k=\frac{6(1-\varepsilon)}{\varepsilon}\frac{D}{d_p^2}\Bigg/\left[\frac{1}{Sh}+\frac{1}{\varepsilon_{part}^2}\left(\frac{1}{z^{1/3}}-1\right)\right]. \tag{24}$$

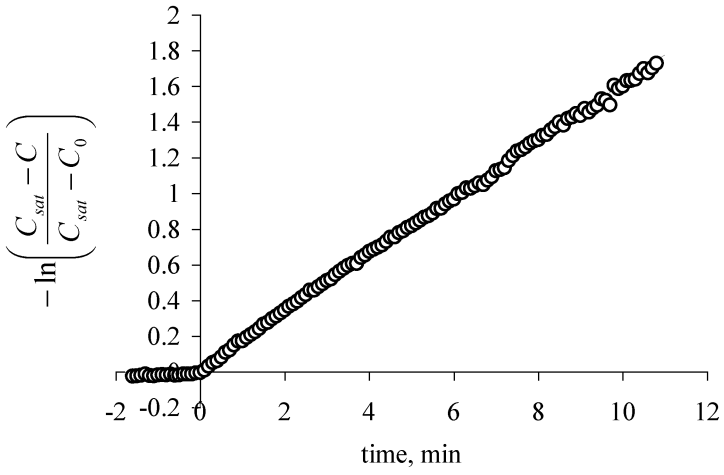

Fig. 11. Mass transfer from bed to freeboard was calculated from the rate at which concentrations increased in the freeboard after gas flow was stopped. (Here, liquid loading was 0.57 and $\omega = 0.266\ s^{-1}$.)

Table 4
Parameters used for the modelling of our data

Parameter	Value
Binary diffusion coefficient, pentanol–air (D)	$8.25 \times 10^{-6}\ m^2 s^{-1}$
Kiln radius	0.075 m
Fill fraction	0.27
Bed porosity (ε)	0.636
Particle porosity (ε_{part})	0.15
Particle diameter (d_p)	0.016 m
Sherwood number (Sh)	3.8

The effective dispersion coefficient within the particle was estimated as $\varepsilon_{part}^2 D$, and the value of ε_{part} (0.15) was inferred from the experimental data taken at the slowest drying rates. The parameters used in the model are given in Table 4.

The total depletion model was not applicable at these experimental conditions, so η was estimated using Eq. (12), and k was estimated from Eq. (24). This enabled us to plot our model $\eta\varepsilon k$ values with those that we obtained by experiment at the two rotation speeds that the equipment was capable of maintaining (Fig. 12).

The predicted mass transfer rates follow the trend of the experimental data quite well. By using the model prediction of k at the various liquid loadings (Eq. (24)), and using the data $\eta\varepsilon k$ shown in Fig. 12, it is possible to calculate the effectiveness factor η and k/ω at each of the experimental data points. These points (Fig. 13) follow the expected trend quite well, but show some scatter. The experimental data for $0.6 < k/\omega < 2$ were measured with wet pellets, and the values measured for $0.02 < k/\omega < 0.1$ using externally dry pellets are slightly higher than expected, possibly due to uneven drying on the surface of the pellets.

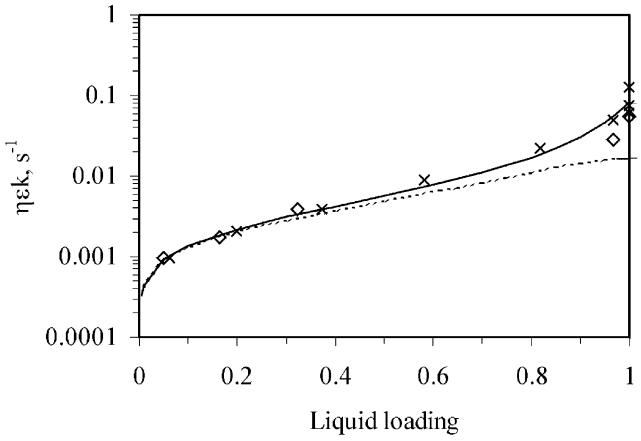

Fig. 12. Characteristic rate is well predicted by the model for both fast rotation (−×−) (0.266 s^{-1}); and slow rotation: (- - -◇- - -) (0.052 s^{-1}).

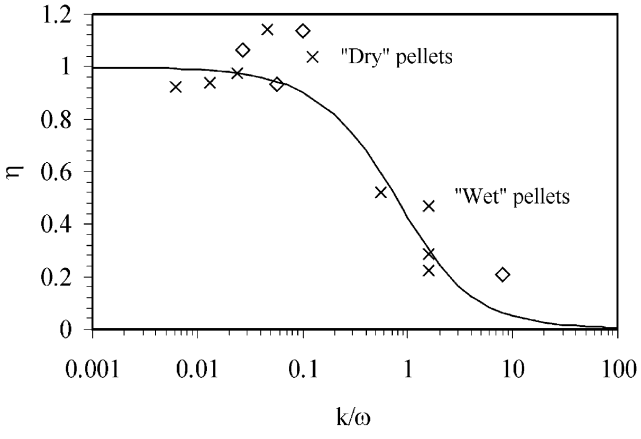

Fig. 13. Effectiveness factors follow the predicted trend as a function of k/ω. (—) Eq. (12): (×) $\omega = 0.266\ s^{-1}$, (◇) $\omega = 0.052\ s^{-1}$.

6. Conclusion

A novel model to predict mass transfer inside a rolling rotary kiln was presented. This model only considers convection inside the voids between the particles inside the bed, which are assumed to be filled with entrapped gas from the freeboard.

The model was found to underestimate mass transfer rates for fast reacting systems ($k/\omega > 2$), especially for the data measured by Jauhari et al. (1998), showing that other mechanisms like dispersion and/or surface phenomena are also important for such systems. Active layer models are to be preferred in these cases. However, for slower reactions ($k/\omega < 2$) the presented model appears to perform much better. It then provides a useful alternative to active layer models, which are clearly inappropriate if the whole bed contributes to mass transfer. For more general applicability, it would be useful to include diffusion/dispersion effects, which will be done in a future paper.

Notation

a	pellet outer surface area per bed volume, m^{-1}
A	bed surface area, m^2
A_x	radial cross-sectional area of the bed, m^{-2}
A_{xg}	radial cross-sectional area of the bed attributable to voidage, (εA_x), m^{-2}
C	Concentration of the evaporating species in the freeboard, mol m^{-3}
C_0	Concentration of the evaporating species in the freeboard at the start of an experiment, when air flow through the freeboard is stopped, mol m^{-3}
C_A	Concentration of species A within the bed, mol m^{-3}
C_{A0}	Concentration of species A within the freeboard, mol m^{-3}
C_{sat}	Concentration of evaporating species at saturation, mol m^{-3}
C_{A0}	Concentration of species A within the freeboard, mol m^{-3}
D	binary diffusion coefficient, m^2 s^{-1}
d_p	particle diameter, m
h	perpendicular distance from radial centre of the kiln to the bed surface, m
k	reaction rate constant, s^{-1}
k_{gs}	mass transfer coefficient on the surface of particles, m s^{-1}
k_s	mass transfer coefficient of active layer, m s^{-1}
L	length of the rotary kiln in axial direction, m
P_A	reaction rate of A, moles m^{-3}(bed) s^{-1}
Q	volumetric gas flow rate, m^3 s^{-1}
R	radius of rotary kiln, m
Sh	dimensionless Sherwood number, dimensionless
r	distance from centre of kiln to the surface of the bed at angle θ or θ_0, m
V	volume, m^3
V_{bed}	volume of bed, m^3
V_f	volume of freeboard, m^3
z	liquid loading in particles: volume of liquid in pores compared to the volume of liquid in pores after being soaked in liquid and wiped dry

Greek letters

ε	bed voidage, m^3(gas) m^{-3}(bed)
ε_{part}	intraparticle porosity, m^3(gas in pores) m^{-3}(pellet)
η	effectiveness factor of reaction
τ	residence time of gas in the bed, s^{-1}
θ	angle, rad
θ_0	starting angle defined in Fig. 5, rad
θ_1, θ_2	angles defined in Figs. 5 and 7, rad
ω	angular velocity, s^{-1}

References

Barr, P. V., Brimacombe, J. K., & Watkinson, A. P. (1989). Heat-transfer model for the rotary kiln: Part II. Development of the cross-section model. *Metallurgical Transactions*, *20B*(3), 403–419.

Heinen, H., Brimacombe, J. K., & Watkinson, A. P. (1983a). Experimental study of transverse bed motion in rotary kilns. *Metallurgical Transactions*, *14B*, 191–205.

Heinen, H., Brimacombe, J. K., & Watkinson, A. P. (1983b). The modelling of transverse bed motion in rotary kilns. *Metallurgical Transactions*, *14B*, 207–220.

Jauhari, R., Gray, M. R., & Masliya, J. H. (1998). Gas–solid mass transfer in a rotating drum. *Canadian Journal of Chemical Engineering*, *76*, 224–232.

Kramers, H., & Crookewit, P. (1952). The passage of granular solids through inclined rotary kilns. *Chemical Engineering Science*, *1*, 259.

Lebas, E. F., Hanrot, F., Ablitzer, D., & Houzelot, J. L. (1995). Experimental study of residence time, particle movement and bed depth profile in rotary kilns. *Canadian Journal of Chemical Engineering*, *73*, 173–179.

Saeman, W. C. (1951). Passage of solids through rotary kilns. *Chemical Engineering Progress*, *47*, 508–514.

Sørensen, J. P., & Stewart, W. E. (1974). Effect of fluid dispersion coefficients on particle-to-fluid mass transfer coefficients in packed beds. *Chemical Engineering Science*, *33*, 1374–1384.

Spurling, R. J., Davidson, J. F., & Scott, D. M. (2000). The no-flow problem for granular material in rotating kilns and dish granulators. *Chemical Engineering Science*, *55*, 2303–2313.

Sullivan, J. D., Maier, C. G., & Ralston, O. C. (1927). Passage of solid particles through rotary cylindrical kilns. US Bureau of Mines, Technical Papers 384 (pp. 1–42).

Tscheng, S. H., & Watkinson, A. P. (1979). Convective heat transfer in a Rotary Kiln. *Canadian Journal of Chemical Engineering*, *57*, 433–443.